1544 *Inorg. Chem.* **2011**, *50*, 1544–1550
DOI: 10.1021/ic102145s

Inorganic Chemistry
Article

$[Mn(C_4H_{10}ON)(H_2O)][Fe(CN)_6]$: A Three-Dimensional Cyanide-Bridged Ferrimagnet with a Morpholine Ligand

Ning Jiang, Feng-Yan Li, Lin Xu,* Li−Li Zhao, and Yu-Chao Wang

Key Laboratory of Polyoxometalates Science of Ministry of Education, College of Chemistry, Northeast Normal University, Changchun 130024, People's Republic of China

Received October 25, 2010

The reaction of the Mn(II) and $[Fe(CN)_6]^{3-}$ ions in the presence of morpholine at 90 °C yields a new cyanide-bridged three-dimensional (3D) assembly, showing a ferrimagnetic ordering, frequency-dependent ac susceptibility, and hysteresis loops below 14.8 K. In addition, our feasible route to rationally design and prepare this new molecule-based ferrimagnet promises to provide new 3D cyanide-bridged complexes in the future research.

Introduction

The rational design and synthesis of molecular magnetic materials exhibiting spontaneous magnetization, to fully understand the magnetostructural correlations, is continuously attracting more and more attention. The strategy is usually involved with the cyanide-bridged materials,[1,2] which are beneficial to extended arrays of high dimensionalities with the higher magnetic ordering temperature[3−5] or the high coercivity,[6−8] because of the increased number of interacting neighbors. The representative example is the three-dimensional (3D) Prussian Blue-type complexes constructed by transition-metal ions and hexacyanometallate(III) building blocks.[9] Within the cyanide family, the cyanide-bridged bimetallic assemblies, especially for the low dimensional $Mn^{II/III}-CN-Fe^{II/III}$ species, have been widely synthesized and deeply studied. To tune the dimensionality of the Mn-CN-Fe cyanide structures, several synthetic strategies have been employed:

(i) The reaction of hexacyanometallate $[Fe^{II/III}(CN)_6]^{n-}$ unit and metal ions $Mn^{2+/3+}$ always results in the 3D networks with high symmetry: $Na_2[Mn^{II}Fe^{II}(CN)_6]$,[10] $Rb_{0.7}Mn^{II}_{1.15}[Fe^{III}(CN)_6]\cdot 2H_2O$,[11a] $RbMn^{II}[Fe^{III}(CN)_6]$,[11b] and $Rb_{0.82}Mn^{II}_{0.20}Mn^{III}_{0.80}[Fe^{II}(CN)_6]_{0.80}[Fe^{III}(CN)_6]_{0.14}\cdot H_2O$.[12] The first one of them shows a three-dimensional (3D) cubic crystal framework analogous to that of the classical Prussian Blue, in which Fe and Mn atoms locate in the cubic vertices, and exhibits a ferrimagnetic ordering with a critical temperature of $T_C = 3.5$ K, a coercive field of $H_C = 330$ Oe, and a remnant magnetization of 503 cm^3 Oe mol^{-1}. The structures of the remaining three complexes were determined by powder X-ray diffraction or elemental analyses, because only powdery samples, instead of single crystalline ones, were obtained.

(ii) To construct low-dimensional species, the following three sensible approaches are usually introduced: the

*To whom correspondence should be addressed. E-mail: linxu@nenu.edu.cn.

(1) (a) Ohba, M.; Ōkawa, H. *Coord. Chem. Rev.* **2000**, *198*, 313–328. (b) Tanase, S.; Reedijk, J. *Coord. Chem. Rev.* **2006**, *250*, 2501–2510.
(2) Marius, A.; Jean-Pierre, C.; Carmen, D.; Gao, S. *Inorg. Chem.* **2009**, *48*, 3342–3359.
(3) Dujardin, E.; Ferlay, S.; Phan, X.; Desplanches, C.; Moulin, C. C. D.; Sainctavit, P.; Baudelet, F.; Dartyge, E.; Veillet, P.; Verdaguer, M. *J. Am. Chem. Soc.* **1998**, *120*, 11347–11352.
(4) Entley, W. R.; Girolami, G. S. *Science* **1995**, *268*, 397–400. (b) Ferlay, S.; Mallah, T.; Ouahès, R.; Veillet, P.; Verdaguer, M. *Nature* **1995**, *378*, 701–703.
(5) Verdaguer, M.; Bleuzen, A.; Marvaud, V.; Vaissermann, J.; Seuleiman, M.; Desplanches, C.; Scuiller, A.; Train, C.; Garde, R.; Gelly, G.; Lomenech, C.; Rosenman, I.; Veillet, P.; Cartier, C.; Villain, F. *Coord. Chem. Rev.* **1999**, *190−192*, 1023–1047.
(6) Kurmoo, M.; Kepert, C. J. *New J. Chem.* **1998**, *22*, 1515–1524.
(7) Manson, J. L.; Kmety, C. R.; Huang, Q. Z.; Lynn, J. W.; Bendele, G. M.; Pagola, S.; Stephens, P. W.; Liable-Sands, L. M.; Rheingold, A. L.; Epstein, A. J.; Miller, J. S. *Chem. Mater.* **1998**, *10*, 2552–2560.
(8) Batten, S. R.; Jensen, P.; Moubaraki, B.; Murray, K. S.; Robson, R. *Chem. Commun.* **1998**, *3*, 439–440.
(9) For example: (a) Kou, H. Z.; Gao, S.; Zhang, J.; Wen, G. H.; Su, G.; Zheng, R. K.; Zhang, X. X. *J. Am. Chem. Soc.* **2001**, *123*, 11809–11810. (b) Verdaguer, M. *Science* **1996**, *272*, 698–699. (b) Sato, O.; Iyoda, T.; Fujishima., A.; Hashimoto, K. *Science* **1996**, *272*, 704–705. (c) Holmes, S. M.; Girolami, G. S. *J. Am. Chem. Soc.* **1999**, *121*, 5593–5594. (d) Hatlevik, Ø.; Buschmann, W. E.; Zhang, J.; Manson, J. L.; Miller, J. S. *Adv. Mater.* **1999**, *11*, 914–918.
(10) Jiang, L.; Feng, X. L.; Lu, T. B.; Gao, S. *Inorg. Chem.* **2006**, *45*, 5018–5026.
(11) (a) Serena, M.; Kosmas, P.; Andrew, N. F. *Angew. Chem., Int. Ed.* **2004**, *43*, 6316–6319. (b) Tokoro, H.; Ohkoshi, S.; Matsuda, T.; Hashimoto, K. *Inorg. Chem.* **2004**, *43*, 5231–5236.
(12) Ohkoshi, S.; Tokoro, H.; Matsuda, T.; Takahashi, H.; Irie, H.; Hashimoto, K. *Angew. Chem., Int. Ed.* **2007**, *46*, 3238–3241.
(13) (a) Thorsten, G.; Maik, H.; Erich, K.; Hartmut, Bögge.; Anja, Stammler.; Roland, Fröhlich.; Eckhard, Bill.; Jürgen, Schnack. *Inorg. Chem.* **2009**, *48*, 607–620. (b) Hitoshi, Miyasaka.; Hidenori, Ieda.; Naohide, Matsumoto.; Nazzareno, Re.; Raffaella, Crescenzi.; Carlo, Floriani. *Inorg. Chem.* **1998**, *37*, 255–263. (c) Shatruk, M.; Chambers, K. E.; Prosvirin, A. V.; Dunbar, K. R. *Inorg. Chem.* **2007**, *46*, 5155–5165. (d) Carmen, P.; Marius, A.; Yves, J.; Zdirad, Z.; Nathalie, K.; Louis, R. *J. Mater. Chem.* **2006**, *16*, 2660–2668.

Published on Web 12/28/2010

$[Fe^{II/III}(CN)_6]^{n-}$ unit combined with $[Mn(L)_x(H_2O)_y]^{m+}$ (L = organic ligand), the use of modified cyanometallates $[Fe^{II/III}(L')_a(CN)_b]^{n-}$ (L′ = polydentate ligands) as the building blocks toward metal ions $Mn^{2+/3+}$, or the combination of $[Fe^{II/III}(L')_a(CN)_b]^{n-}$ and $[Mn(L)_x(H_2O)_y]^{m+}$. So far, all three approaches are used to provide plenty of discrete bimetallic complexes,[10,13−15] one-dimensional (1D) chains,[10,15a−c,16−18,21a,21c,b] and two-dimensional (2D) layers,[16c,19−21] including various single-molecule magnets (SMMs),[22,23a] single-chain magnets (SCMs),[23] ferrimagnets,[24] and ferromagnets,[25] which could probably be used in information storage. Nonetheless, compared to the large number of low-dimensional cyanides (discrete polynuclear species, 1D chains, and 2D layered complexes), the 3D Mn-CN-Fe cyanide-bridged solids possessing single crystals suitable for X-ray diffraction (XRD) analysis are still limited, because of their insolubility and difficulty in single-crystal growth, which, thus, precludes the possibility to investigate the correlation between their crystal structures and their magnetic properties.

Among the 3D cyanides, the face-centered cubic ones always exhibit low or no magnetic coercivity, because of their low or no magnetic anisotropy.[26] In contrast, the noncubic framework with innate anisotropy in structure could efficiently enhance the magnetic anisotropy. Therefore, the exact structure information (from single-crystal XRD) of high-dimensional cyanide-bridged complexes with anisotropic networks (noncubic structures) is of current significance for supplying suitable models to reveal the magnetostructural correlation.

The use of the stable and economical cyanide salt, $K_3Fe^{III}(CN)_6$ with transition-metal cations, is an efficient way for constructing the novel 3D cyanides needed to enrich the database of 3D cyanides and promote our comprehension of their magnetostructural correlation. However, the fast reactions between the $[Fe^{III}(CN)_6]^{3-}$ trianion and transition-metal cations facilely form amorphous, powdery, or microcrystalline solids but not single crystals. Therefore, how to obtain XRD-quality single crystals, which makes the structure determination of complexes easier, is a rather tough task to fulfill. We have performed some trials in synthesizing 3D cyanide-bridged complexes, using organic amines such as imidazole, pyridine, and morpholine as both the coordinated ligand and the charged counterion. When using morpholine, we obtained the XRD-quality single crystals of a novel 3D cyanide-bridged complex $[Mn(C_4H_{10}ON)(H_2O)][Fe(CN)_6]$ (**1**), which was well-confirmed by XRD and characterized through magnetic measurements. To the best of our knowledge, complex **1** is the first case of 3D noncubic architecture constructed by the $Fe^{III}-CN-Mn^{II}-NC$ linkages. Below the critical temperature (T_C = 14.8 K), complex **1** exhibits long-range ferrimagnetic ordering, frequency-dependent real and imaginary phases caused by the spin glass behavior, and the high coercive field (1119 Oe) with large remnant magnetization (6153 $cm^3\ mol^{-1}$ Oe). Note that the critical temperature of complex **1** is highest in the $Fe^{III}-Mn^{II}$ cyanides so far. Moreover, the magnetostructural correlation is concluded in this paper after the comparison between our complex and the reported Fe−Mn cyanides.

Experimental Section

All chemicals were commercially purchased and used without further purification.

Preparation of $[Mn(C_4H_{10}ON)(H_2O)][Fe(CN)_6]$ (1). Morpholine (0.45 mL, 5.16 mmol) and $Mn(CH_3COO)_2\cdot 4H_2O$ (0.0794 g, 0.233 mmol) were added to the 1 M NaCl water solution (20 mL). The mixture was then acidified to pH 2.5−5.5, using 6 M HCl, followed by the addition of $K_3[Fe(CN)_6]$ (0.0888 g, 0.27 mmol). The resulting reaction mixture was heated to 90 °C for 1 h and then cooled to room temperature. Undisturbed evaporation of the solvent for one week at room temperature generated the brown crystals suitable for X-ray single diffraction analysis (yield: 22 mg, 0.059 mmol, 25% based on Mn). Elemental analysis, calcd (%): Fe 14.97, M_n 14.73, C 32.20, N 26.28, H 3.24; found: Fe 14.78, M_n 14.86, C 32.02, N 26.07, H 3.47.

(14) (a) Lescouëzec, R.; Lloret, F.; Julve, M.; Vaissermann, J.; Verdaguer, M. *Inorg. Chem.* **2002**, *41*, 818–826. (b) Wang, S.; Zuo, J. L.; Zhou, H. C.; Song, Y.; Gao, S.; You, X. Z. *Eur. J. Inorg. Chem.* **2004**, 3681–3687.

(15) (a) Kim, J. I.; Yoo, H. S.; Koh, E. K.; Hong, C. S. *Inorg. Chem.* **2007**, *46*, 10461–10463. (b) Kim, J. I.; Kwak, H. Y.; Yoon, J. H.; Ryu, D. W.; Yoo, I. Y.; Yang, N.; Cho, B. K.; Park, J. G.; Lee, H.; Hong, C. S. *Inorg. Chem.* **2009**, *48*, 2956–2966. (c) Li, D. F.; Parkin, S.; Wang, G. B.; Yee, G. T.; Holmes, S. M. *Inorg. Chem.* **2006**, *45*, 1951–1959. (d) Ni, Z. H.; Kou, H. Z.; Zheng, L.; Zhao, Y. H.; Zhang, L. F.; Wang, R. J.; Cui, A. L.; Sato, Osamu. *Inorg. Chem.* **2005**, *44*, 4728–4736. (e) Luminita, M. T.; Rodrigue, L.; Liviu, D. T.; Francesc, L.; Miguel, J.; Jacqueline, V.; Marius, A. *J. Chem. Soc., Dalton Trans.* **2002**, 3171–3176. (f) Ni, Z. H.; Kou, H. Z.; Zhang, L. F.; Ni, W. W.; Jiang, Y. B.; Cui, A. L.; Ribas, J.; Sato, O. *Inorg. Chem.* **2005**, *44*, 9631–9633. (g) Kwak, H. Y.; Ryu, D. W.; Kim, H. C.; Koh, E. K.; Cho, B. K.; Hong, C. S. *Dalton Trans.* **2009**, *11*, 1954–1961.

(16) (a) Parker, R. J.; Spiccia, L.; Moubaraki, B.; Murray, K. S.; Hockless, D. C. R.; Rae, A. D.; Willis., A. C. *Inorg. Chem.* **2002**, *41*, 2489–2495. (b) Lescouëzec, R.; Vaissermann, J.; Toma, L. M.; Carrasco, R.; Lloret, F.; Julve, M. *Inorg. Chem.* **2004**, *43*, 2234–2236. (c) Hitoshi, M.; Naohide, M.; Nazzareno, R.; Emma, G.; Carlo, F. *Inorg. Chem.* **1997**, *36*, 670–676.

(17) (a) Lescouëzec, R.; Lloret, F.; Julve, M.; Vaissermann, J.; Verdaguer, M.; Llusar, R.; Uriel, S. *Inorg. Chem.* **2001**, *40*, 2065–2072. (b) Wang, S.; Ferbinteanu, M.; Yamashita, M. *Inorg. Chem.* **2007**, *46*, 610–612. (c) Wen, H. R.; Wang, C. F.; Zuo, J. L.; Song, Y.; Zeng, X. R.; You, X. Z. *Inorg. Chem.* **2006**, *45*, 582–590.

(18) (a) Hayami, S.; Juhász, G.; Maeda, Y.; Yokoyama, T.; Sato, O. *Inorg. Chem.* **2005**, *44*, 7289–7291. (b) Kim, J. I.; Yoo, H. S.; Koh, E. K.; Kim, H. C.; Hong, C. S. *Inorg. Chem.* **2007**, *46*, 8481–8483.

(19) (a) Bonadio, Federica.; Senna, M. C.; Ensling, J.; Sieber, A.; Neels, A.; Stoeckli-Evans, H.; Decurtins, S. *Inorg. Chem.* **2005**, *44*, 969–978. (b) Miyasaka, H.; Okawa, H.; Miyazaki, A.; Enoki, T. *Inorg. Chem.* **1998**, *37*, 4878–4883. (c) Smith, J. A.; Galán-Mascarós, J. R.; Clérac, R.; Dunbar, K. R. *Chem. Commun.* **2000**, 1077–1078.

(20) Kim, J.; Han, S.; Pokhodnya, K. I.; Migliori, J. M.; Miller, J. S. *Inorg. Chem.* **2005**, *44*, 6983–6988.

(21) (a) Kim, J. I.; Yoon, J. H.; Kwak, H. Y.; Koh, E. K.; Hong, C. S. *Eur. J. Inorg. Chem.* **2008**, 2756–2763. (b) Clemente-León, M.; Coronado, E.; Galán-Mascarós, J. R.; Gómez-García, C. J.; Woike, T.; Clemente-Juan, J. M. *Inorg. Chem.* **2001**, *40*, 87–94. (c) Zhao, C. C.; Ni, W. W.; Tao, J.; Cui, A. L.; Kou, H. Z. *CrystEngComm* **2009**, *11*, 632–637.

(22) (a) Choi, H. J.; Sokol, J. J.; Long, J. R. *Inorg. Chem.* **2004**, *43*, 1606–1608. (b) Miyasaka, H.; Takahashi, H.; Madanbashi, T.; Sugiura, K.; Clérac, R.; Nojiri, H. *Inorg. Chem.* **2005**, *44*, 5969–5971. (c) Ababei, R.; Li, Y. G.; Roubeau, O.; Kalisz, M.; Bréfuel, N.; Coulon, C.; Harté, E.; Liu, X. T.; Mathonière, C.; Clérac, R. *New J. Chem.* **2009**, *33*, 1237–1248. (d) Li, D. F.; Parkin, S.; Wang, G. B.; Yee, G. T.; Prosvirin, A. V.; Holmes, S. M. *Inorg. Chem.* **2005**, *44*, 4903–4905. (e) Ni, Z. H.; Zhang, L. F.; Tangoulis, V.; Wernsdorfer, W.; Cui, A. L.; Sato, O.; Kou, H. Z. *Inorg. Chem.* **2007**, *46*, 6029–6037.

(23) (a) Ferbinteanu, M.; Miyasaka, H.; Wernsdorfer, W.; Nakata, K.; Sugiura, K.; Yamashita, M.; Coulon, C.; Clérac, R. *J. Am. Chem. Soc.* **2005**, *127*, 3090–3099. (b) Kou, H. Z.; Ni, Z. H.; Liu, C. M.; Zhang, D. Q.; Cui, A. L. *New J. Chem.* **2009**, *33*, 2296–2299.

(24) (a) Wen, H. R.; Wang, C. F.; Li, Y. Z.; Zuo, J. L.; Song, Y.; You, X. Z. *Inorg. Chem.* **2006**, *45*, 7032–7034. (b) Miyasaka, H.; Ieda, H.; Matsumoto, N.; Sugiura, K.; Yamashita, M. *Inorg. Chem.* **2003**, *42*, 3509–3515.

(25) (a) Nazzareno, R.; Emma, G.; Carlo, F.; Hitoshi, M.; Naohide, M. *Inorg. Chem.* **1996**, *35*, 6004–6008. (b) Ni, W. W.; Ni, Z. H.; Cui, A. L.; Liang, X.; Kou, H. Z. *Inorg. Chem.* **2007**, *46*, 22–33.

(26) Kou, H. Z.; Gao, S.; Ma, B. Q.; Liao, D. Z. *Chem. Commun.* **2000**, *14*, 1309–1310.

X-ray Crystallography. For the single-crystal structure determination, crystal data of **1** were measured on a CrysAlisPro CCD system (Oxford Diffraction), using Mo Kα radiation (λ = 0.71073 Å) at 293(2) K. The structure was solved with the direct methods (SHELXS-97) and refined on F^2 by full-matrix least-squares (SHELXL-97).[27] (CCDC-763573 contains the supplementary crystallographic data for this paper. The data can be obtained free of charge from the Cambridge Crystallographic Data Centre via www.ccdc.cam.ac.uk/data_request/cif.)

Physical Measurements. Elemental analyses (Fe and Mn) were determined by a Leaman inductively coupled plasma (ICP) spectrometer. Elemental analyses (C, H, and N) were performed on a Perkin−Elmer Model 2400 CHN elemental analyzer. The infrared spectrum of the solid sample was obtained on a BRUKER Model Vertex 70 FTIR spectrometer in the 400−4000 cm^{-1} region with a KBr pellet. Thermogravimetric (TG) analysis was performed on a Perkin−Elmer Model TGA7 instrument in the flowing N_2 atmosphere at the heating rate of 10 °C min^{-1}. Magnetic susceptibility data were recorded using a Quantum Design SQUID MPMS XL-5 magnetometer. Variable-temperature susceptibility measurements were performed in the temperature range of 2−300 K, under a magnetic field of 1000 Oe on polycrystalline samples. The experimental susceptibilities were corrected for the diamagnetism of the constituent atoms (Pascal's constants).

Results and Discussion

Synthesis. The aqueous solution reaction of the Mn(II) ion and the building block $[Fe(CN)_6]^{3-}$ ion in the presence of morpholine at 90 °C produced a brown solution, from which brown blocklike crystals were obtained by slow evaporation without disturbance. Our motivation is to conduct the formation of 3D Mn-CN-Fe cyanide materials[10−12] via the reaction of the hexacyanometallate $[Fe^{II/III}(CN)_6]^{n-}$ unit with metal ions $Mn^{2+/3+}$. However, there were two disadvantages in the conventional strategy for synthesizing 3D noncubic framework. First, the conventional approach, using noncoordinated counterions (such as alkali-metal ions), is likely to result in the 3D networks of cubic symmetry. Second, those fast reactions in the conventional approach counteract the formation of single crystals. Therefore, the introduction of an assistant ligand is beneficial to break the cubic symmetry and obtain single crystals with noncubic 3D structures. Apparently, the chelate ligands, which are usually used in synthesizing low-dimensional cyanide-bridged assemblies, are not suitable for synthesizing 3D cyanides. Instead, we used imidazole, pyridine, and morpholine as assistant ligands to act as both the coordinated ligand and the charged counterion. Using morpholine as an assistant ligand, we obtained XRD-quality single crystals of the title complex. Different from the approach of slow diffusion through aqueous or nonaqueous solvents that were usually used in synthesizing cyanide-bridged assemblies, the reaction for **1** was operated in the aqueous solution at relatively high temperature (90 °C). Although the high temperature favors the formation of insoluble 3D cyanometallate powder, the introduction of morpholine molecules effectively reduces the quantity of deposition herein. The morpholine could inhabit the coordination sites of Mn^{II} via the oxygen atom to protect the transition-metal ions against constructing the 3D cyanometallate too quickly and, consequently, reduce the quantity of deposition. Furthermore, the protonated morpholine molecules under the synthetic conditions balance the charge of the repeating unit in the polymeric framework, which plays an assistant counterion role in the formation of a 3D architecture. In addition, the similar reactions with imidazole and pyridine offered powdery solids, rather than crystalline ones. The probable reasons are as follows:

(1) Imidazole molecules are smaller than morpholine molecules in size, which may not be suitable to hold the 3D cyanide structures in this system.

(2) After protonation, although the pyridine molecule possesses the similar size with morpholine, it is the lack of coordination sites that seems to be very significant in the crystallization process. Thus, only the reaction involving the protonated morpholine molecules with the suitable size and the residual coordination sites could afford the single crystals for the measurement.

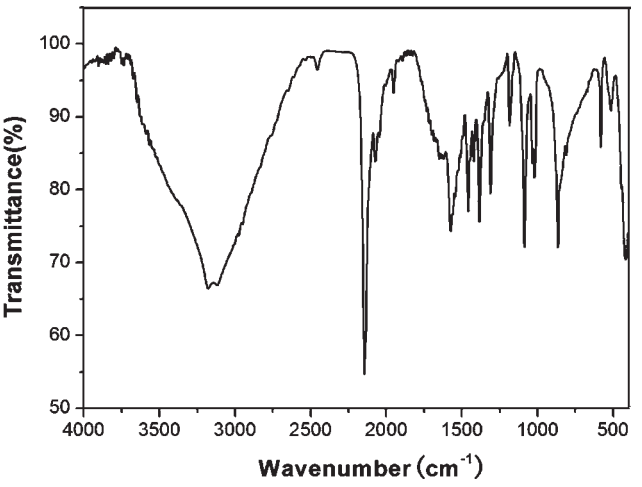

Figure 1. Infrared (IR) spectrum of **1**.

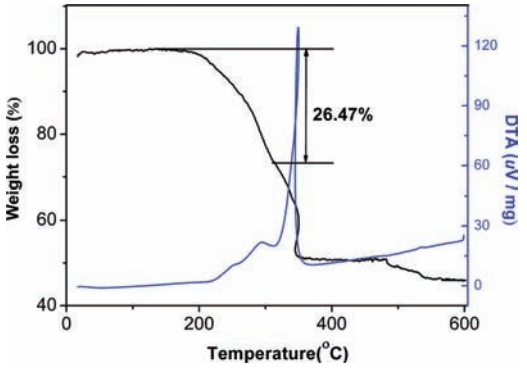

Figure 2. Thermogravimetric analysis (TGA) data for **1**.

IR Spectroscopy and Thermogravimetric Analysis. The new bimetallic compound shows two ν(C≡N) modes at 2146 and 2073 cm^{-1} (see Figure 1). The IR band at 2146 cm^{-1} can be contributed to the bridging cyanide group, while the ν(C≡N) mode at 2073 cm^{-1} is attributed to the terminal cyanide group.[28] Thermal stability of complex **1** was studied using thermogravimetric analysis (TGA) (see Figure 2). The TGA of **1** shows a continuous mass loss of

(27) Sheldrick, G. M. *SHELXS97 and SHELXL97*; University of Göttingen: Göttingen, Germany, 1997.

(28) Ohba, M.; Ōkawa, H.; Fukita, N.; Hashimoto, Y. *J. Am. Chem. Soc.* **1997**, *119*, 1011–1019.

Table 1. X-ray Crystallographic Data for **1**

formula	$C_{10}H_{12}FeMnN_7O_2$
M_r [g]	373.06
crystal size (mm)	0.25 × 0.25 × 0.25
crystal system	orthorhombic
space group	*Pnma*
Z	4
a [Å]	13.6311(4)
b [Å]	13.3758(4)
c [Å]	8.5310(3)
V [Å^3]	1555.43(9)
D_c [g cm^{-3}]	1.593
μ [mm^{-1}]	1.758
reflections collected	1429
refined parameters	106
R_1 [$I > 2\sigma(I)$][a]	0.0235
wR_2 [all data][b]	0.0461
GOF on F^2	0.999
largest diff. peak/hole [e Å^{-3}]	0.231/−0.434

[a] $R_1 = \sum||F_0| - |F_c||/\sum|F_c|$. [b] $wR_2 = [\sum w(F_0^2 - F_c^2)^2/\sum w(F_0^2)^2]^{1/2}$ with $1/w = \sigma^2F_0^2 + aP^2 + bP$ and $P = F_0^2 + 2F_c^2/3$.

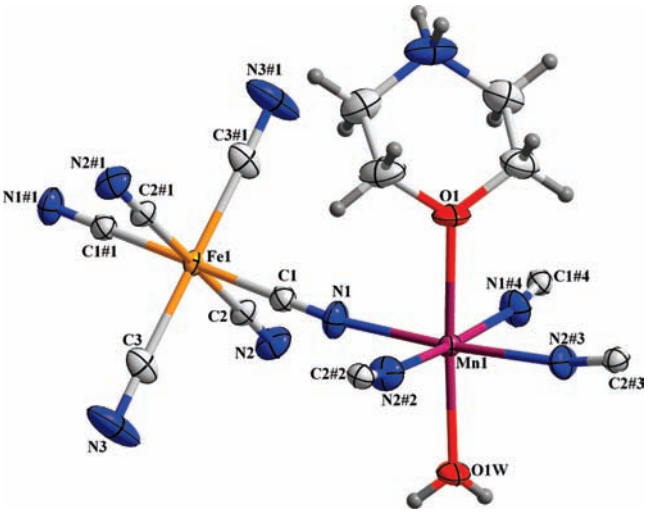

Figure 3. ORTEP diagram of **1** (50% probability for the ellipsoids). Symmetry codes: #1 = (−x,−y,1 − z); #2 = (0.5 + x,y, 0.5 − z); #3 = (0.5 + x,0.5 − y,0.5 − z); #4 = (x,0.5 − y,z).

26.47% from 172 °C to 312 °C (DTG_{max} = 251 and 292 °C), corresponding to the removal of one coordinated water molecular and one coordinated morpholine molecular from the formula unit $[Mn(C_4H_{10}ON)(H_2O)][Fe(CN)_6]$ (calcd, 28.45%). After 312 °C, complex **1** immediately decomposes with further heating.

Crystal Structure. Complex **1** crystallizes in the orthorhombic *Pnma* space group (see Table 1). As shown in Figure 3, the asymmetric unit consists of one Mn^{II} dication, one protonated morpholine monocation, one $[Fe^{III}(CN)_6]^{3-}$ trianion, and one water molecule.

For Fe(1), the equatorial plane is defined by the [C(1), C(1)#1, C(2), C(2)#1] donor set from four cyanide groups and the axial sites are occupied by [C(3), C(3)#1] (the bond angle of C−Fe−C is 180°) from two cyanide groups. The Fe(III) ion occupies the special position (Fe (0,0,$^1/_2$)), possessing a slightly distorted octahedron geometry. The distances of Fe−C are 1.942(2), 1.939(2), and 1.929(3) Å for Fe(1)−C(1), Fe(1)−C(2), and Fe(1)−C(3), respectively. The Fe^{III}−C bond lengths are consistent with the literature[13c,19a] value (1.92−1.95 Å) given for the Fe^{III}−C−N−Mn^{II} system. The angle Fe−C−N is almost linear (178.8°, on average).

Table 2. Selected Bond Distances and Bond Angles for Complex **1**

bond	length (Å)	bond angle	measurement (°)
Fe(1)−C(3)	1.929(3)	C(2)−Fe(1)−C(1)	89.62(9)
Fe(1)−C(2)	1.939(2)	C(3)−Fe(1)−C(1)	88.5(1)
Fe(1)−C(1)	1.942(2)	C(3)−Fe(1)−C(2)	87.45(9)
Mn(2)−N(1)	2.202(2)	N(1)−C(1)−Fe(1)	179.8(2)
Mn(2)−N(2)	2.224 (2)	N(2)−C(2)−Fe(1)	177.9(2)
		N(3)−C(3)−Fe(1)	178.6(3)
		N(1)−Mn(2)−N(1)#4	89.5(1)
		N(1)−Mn(2)−N(2)#3	175.08(8)
		N(1)#4−Mn(2)−N(2)#3	91.72(7)
		N(2)#3−Mn(2)−N(2)#2	86.6(1)
		C(2)−N(2)−Mn(2)#5	167.8(2)
		C(1)−N(1)−Mn(2)	169.9(2)

[a] Symmetry transformations used to generate equivalent atoms: #2 = (0.5 + x,y,0.5 − z); #3 = (0.5 + x,0.5 − y,0.5 − z); #4 = (x,0.5 − y,z); #5 = (x − 0.5,y,−z + 0.5).

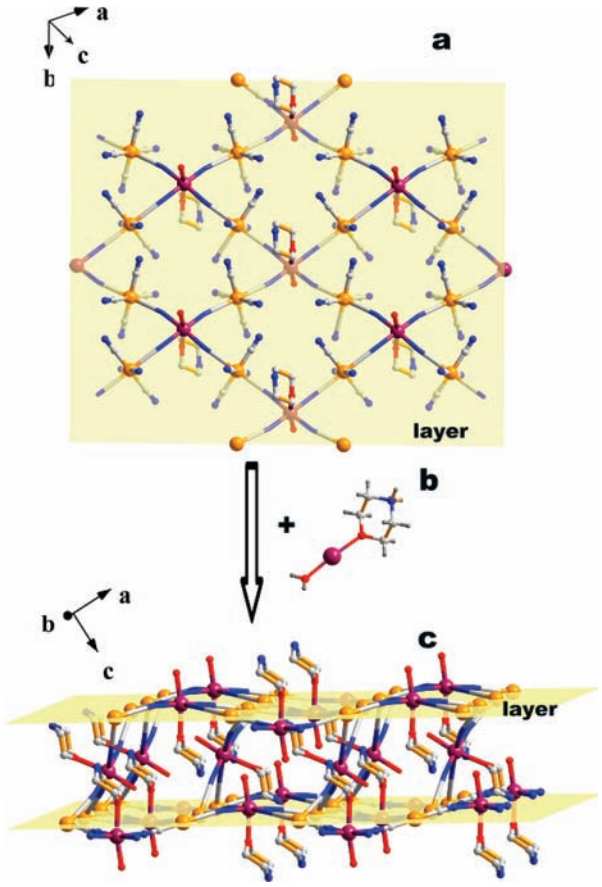

Figure 4. (a) Gridlike layers of complex **1** (Fe atoms are shown as orange, Mn atoms are shown as plum, O atoms are shown as red, N atoms are shown in blue, and C atoms are shown in gray; for the sake of clarity, H atoms are omitted). (b) The connector $[Mn(C_4H_{10}ON)(H_2O)]^{3+}$ units. (c) The 3D network structure of **1**.

The Mn(II) ion possesses a slightly distorted N_4O_2 octahedron geometry. For Mn(1), the equatorial plane is occupied by the [N(1), N(2)#2, N(2)#3, N(1)#4] donor set from four cyanide groups of four $[Fe^{III}(CN)_6]^{3-}$ anions and the axial sites are inhabited by [O(1), O(1)W] from one protonated morpholine monocation and one water molecule. The distances of Mn−N are 2.202(2) and 2.224(2) Å for Mn(1)−N(1) and Mn(1)−N(2), respectively, while the Mn−O distances are 2.252(2) and 2.135(3) Å for Mn(1)−O(1) and Mn(1)−O(1)W, respectively.

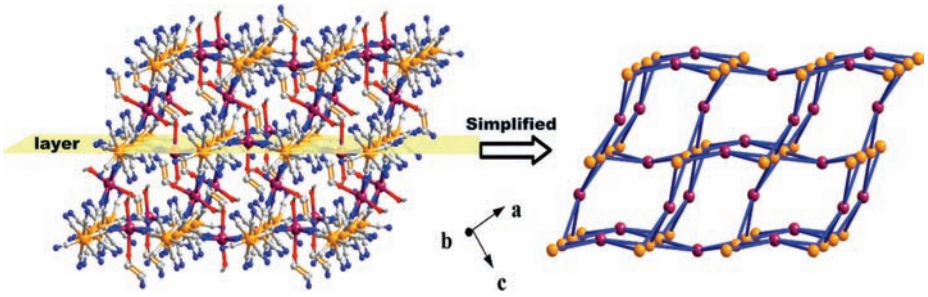

Figure 5. Schematic showing the packing structure and its simplified polygon network topology of complex **1** (only considering Fe (orange) and Mn (plum) atoms as nodes, the Fe−Mn separations are < 5.30 Å).

Bond valence sum (BVS) calculations[29] indicate that the manganese center exhibits a 2+ oxidation state. The bond angle of O−Mn−O is 170.11°. The bridged Mn−N−C linkages are slightly bent [167.8° and 169.9°]. The selected bond lengths and angles for **1** are listed in Table 2.

Each Fe(III) ion connects four Mn(II) ions through four equatorial cyanide ligands, while each Mn(II) ion also connects with four neighboring Fe(III) ions via four cyanide ligands. The Fe^{III}−Mn^{II} separations through μ_2−CN bridges are 5.270 and 5.269 Å for Fe(1)···Mn(1) and Fe(1)···Mn(1)#5, respectively (#5 represents the symmetry transformation used to generate equivalent atoms: $0.5 - x, -y, 0.5 + z$). The shortest Fe^{III}···Fe^{III} and Mn^{II}···Mn^{II} separations are 6.688 Å and 6.905 Å, respectively. As shown in Figure 4, the resulting 3D network can be described as follows. Two *trans*-CN ligands around the Fe(III) atom coordinate with two $[Mn(C_4H_{10}ON)(H_2O)]^{3+}$ units, while the Mn atom connects four $[Fe(CN)_6]^{3-}$ groups, which leads to a 2D corrugated gridlike layer (see Figure 4a). The adjacent 2D layers are further interconnected by the $[Mn(C_4H_{10}ON)(H_2O)]^{3+}$ units (see Figure 4b) via another two *trans*-CN ligands around the Fe(III) atom to form a unique 3D framework (see Figure 4c). When both of the Fe and Mn atoms are treated as four-connected nodes, this 3D architecture exhibits a (4, 4)-connected network (see Figure 5).

Magnetic Properties. The magnetic susceptibility of **1** was measured on the polycrystalline sample under a field of 1000 Oe in the temperature range of 2−300 K. As shown in Figure 6, the $\chi_m T$ value of **1** at room temperature is 4.83 cm^3 K mol^{-1} per MnFe unit (6.22 μ_B), which is consistent with the spin-only value for one low-spin Fe^{III} ($g_{Fe} = 2.00$, $S_{Fe} = {}^1/_2$) and one high-spin Mn^{II} ions ($g_{Mn} = 2.00$, $S_{Mn} = {}^5/_2$) (4.75 cm^3 K mol^{-1} corresponding to 6.16 μ_B). Upon cooling, the $\chi_m T$ value decreases smoothly to a minimum of 4.05 cm^3 K mol^{-1} at 28 K. Between 28 and 300 K, the χ_m^{-1} vs T data can be fitted to the Curie−Weiss law with $C = 4.95$ cm^3 K mol^{-1} and $\theta = -8.81$ K (see the inset of Figure 6). The obtained Curie constant is in good agreement with the predicted spin-only value for one low-spin Fe^{III} center and one high-spin Mn^{II} center (4.75 cm^3 K mol^{-1}). The small negative Weiss constant indicates that the dominant interactions are weak antiferromagnetic between 28 and 300 K, because of the overlap of the t_{2g} orbitals on both Mn(II) and Fe(III) ions through the CN bridges.[13] Below 28 K, the $\chi_m T$ value abruptly increases to reach a maximum of

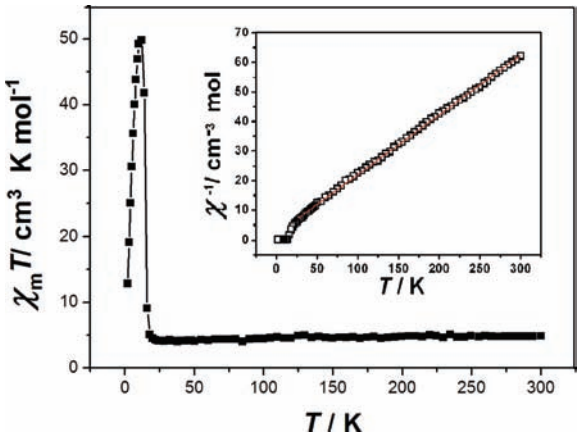

Figure 6. Plot of the temperature dependence of $\chi_m T$ vs T for **1**. The plot of χ_m^{-1} vs T for **1** is shown in the inset (the red solid line represents the best theoretical fit of the data; see text).

49.8 cm^3 K mol^{-1} at 12 K, indicating the onset of the ferrimagnetic ordering. Finally, the $\chi_m T$ value decreases again to 12.9 cm^3 K mol^{-1} at 2 K. The sudden decrease in $\chi_m T$ below 12 K is attributed to the presence of zero-field splitting[14] or the magnetic field saturation effect.

To further confirm the critical temperature for the magnetic ordering, the temperature dependences of the FCM (field-cooled magnetization) and the ZFCM (zero-field-cooled magnetization) were measured under a low field of 50 Oe from 2 K to 50 K (see Figure 7). The divergence of the FCM and ZFCM plots below 14 K reveals the onset of a long-range ferrimagnetic ordering. The derivative curve (d(FCM)/dT) presents an extreme at ~15 K, also corresponding to the critical temperature (Figure 7, inset). The ZFC has a negative magnetization below 11 K, which could be explained by the different ordering temperatures of Fe^{III} (ordered ferromagnetically) and Mn^{II} (ordered antiferromagnetically) magnetic moments and magnetic anisotropy induced by the noncubic structure.[30] Since the ordered magnetic moment of the antiferromagnetic Mn^{II} is larger than that of the ferromagnetic Fe^{III} below 11 K, the total magnetization becomes negative. The magnetocrystalline anisotropy prevents the total magnetization to flip along the applied field direction below 11 K, which plays an important role in achieving the negative magnetization in **1**. The theoretical calculations based on molecular-field theory also predicted the negative magnetization in the Prussian Blue

(29) Brown, I. D.; Altermatt, D. *Acta Crystallogr., Sect. B: Struct. Sci.* **1985**, *B41*, 244.

(30) Kumar, A.; Yusuf, S. M.; Keller, L. J.; Yakhmi, V. *Phys. Rev. Lett.* **2008**, *101*, 207206(1)–207206(4).

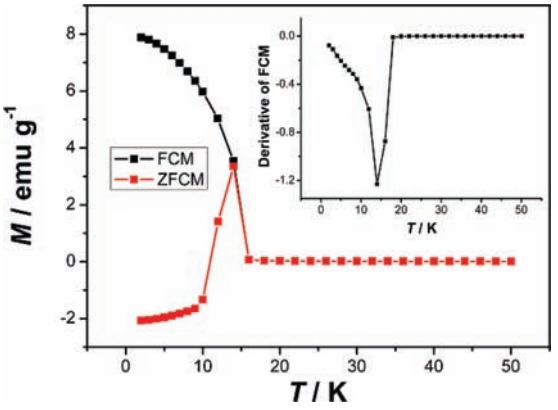

Figure 7. The plots of field-cooled magnetization (FCM) and zero-field-cooled magnetization (ZFCM) for **1**. The derivative of FCM is shown in the inset.

analogues (PBAs).[31−33] The crossover of the FCM from positive to negative below its magnetic ordering temperature would have potential application in the memory device.

To investigate the dynamics of the magnetization of the spontaneous magnetic behaviors, alternating current (ac) susceptibility measurements were performed for **1** under a zero-dc field and a 3 Oe oscillating field in the frequency range of 1−1000 Hz. As shown in Figure 8, the peaks in χ' and χ'' vs T plots in the temperature range of 14.3−14.9 K suggest the existence of a long-range ordered state with a spontaneous magnetic moment at ca. 14.8 K. A slightly temperature dependence of both real (χ') and imaginary (χ'') ac magnetic susceptibilities is observable between 13 K and 16 K. The shift parameter, $\phi = (\Delta T_p/T_p)/\Delta(\log f)$, is ∼0.005, which is close to a typical value for a spin glass.[34]

To further magnetically investigate complex **1**, the field dependences of the magnetization for **1** were measured at 2, 5, 10, 20, and 100 K (see Figure 9). The slopes of the curve increase abruptly from 0 to ca. 4500 Oe below the T_C temperature, while such inflection cannot be observed in the curve above the T_C temperature. Upon increasing the applied magnetic field at 2 K, the magnetization value increases rapidly to 1.26 $N\beta$ at ∼4500 Oe, and then increases linearly to 2.73 $N\beta$ at 50 kOe. Because the saturation magnetization M_S is expected to be 4 $N\beta$ for the system (S_{Mn}, S_{Fe}) = ($^5/_2$, $^1/_2$), based on the equation $M_S = N\mu_B(g_{Fe}S_{Fe} - g_{Mn}S_{Mn})$ for antiferromagnetic coupling, the magnetization has not yet been saturated, even at 50 kOe. The nonsaturation may result from two cases: (1) the presence of a zero-field splitting caused the magnetization to increase more slowly, to reach saturation at much higher fields;[35] or (2) there may be a complicated magnetic structure in which the competition between magnetic interactions with spin canting occurred.[19c]

Hysteresis loops are observed for **1** (see Figure 10), indicating the existence of a ferromagnetic order below its

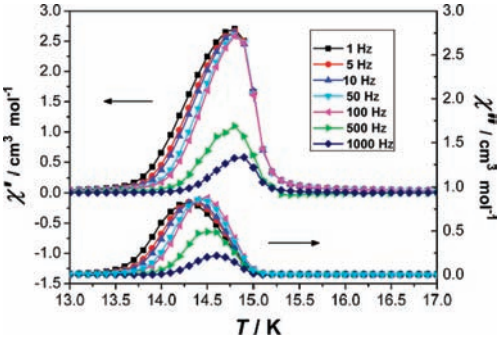

Figure 8. Real (χ') and imaginary (χ'') ac magnetic susceptibilities in an ac field of 3 Oe at different frequencies for **1**.

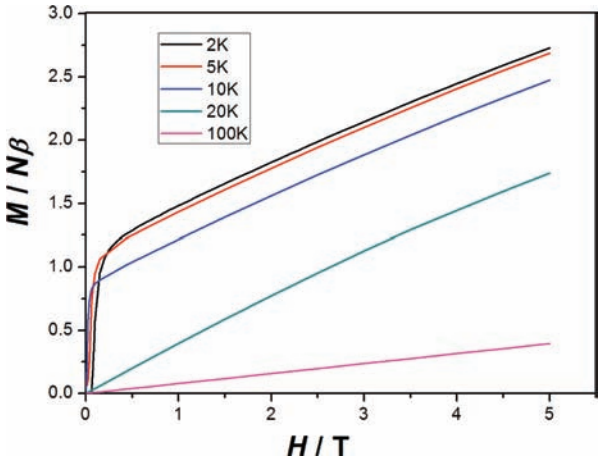

Figure 9. Magnetization versus magnetic field at 2, 5, 10, 20, and 100 K for **1**.

critical temperature in such cyanide-bridged magnetic systems. The values of the coercive field and remnant magnetization are strongly dependent on the temperature. The hysteresis loop observed at 2 K has a coercive field of 1119 Oe and a remnant magnetization of 6153 cm^3 mol^{-1} Oe, which is typical of a hard magnet. Even at 10 K, the hysteresis loop can be still observed with a coercive field of 250 Oe and a remnant magnetization of 1348 cm^3 mol^{-1} Oe.

The antiferromagnetic coupling through the cyanide bridges results from the presence of a net overlap of the magnetic orbitals through the $\pi(t_{2g} - t_{2g})$ pathways ($t_{2g}^3e_g^2$ and $t_{2g}^5e_g^0$ configurations for Mn^{II} and Fe^{III}), while the ferromagnetic term is due to the $\sigma-\pi(t_{2g} - e_g)$ orthogonal coupling.[21c] Such a 3D framework of **1** is a more favorable condition than those low-dimensional species to the $\sigma-\pi$-$(t_{2g} - e_g)$ orthogonal coupling, leading to the ferromagnetic interaction. The magnetic exchange integral (J) between Mn(II) and Fe(III) through the cyanide bridges can be estimated from the expression derived by Verdaguer et al., based on Néel's molecular field theory, as given below:[36]

$$T_C = \left(\frac{|J|}{N\beta^2 g^2 k_B}\right)[Z_{Mn}S_{Mn}(S_{Mn}+1)\cdot Z_{Fe}S_{Fe}(S_{Fe}+1)]^{1/2}$$

(31) Ohkoshi, S. I.; Iyoda, T.; Fujishima, A.; Hashimoto, K. *Phys. Rev.* **1997**, *B56*, 11642.
(32) Ohkoshi, S. I.; Abe, Y.; Fujishima, A.; Hashimoto, K. *Phys. Rev. Lett.* **1999**, *82*, 1285.
(33) Ohkoshi, S. I.; Arai, K.; Sato, Y.; Hashimoto, K. *Nat. Mater.* **2004**, *3*, 857.
(34) Mahata, P.; Natarajan, S.; Panissod, P.; Drillon, M. *J. Am. Chem. Soc.* **2009**, *131*, 10140–10150.
(35) Nazzareno, R.; Emma, G.; Carlo, F.; Hitoshi, M.; Naohide, M. *Inorg. Chem.* **1996**, *35*(21), 6004–6008.
(36) (a) Verdaguer, M.; Bleuzen, A.; Train, C.; Grade, R.; Fabrizi De Biani, F.; Desplanches, C. *Philos. Trans. R. Soc. London, A* **1999**, *357*, 2959. (b) Néel, L. *Ann. Phys. Paris* **1948**, *3*, 137–198.

Table 3. Reported Experimental Magnetic Behaviors with Critical Temperature (T_C), Coercive Field, and Remnant Magnetization for 3D and 2D $Mn^{II}Fe^{III}$-Type Prussian Blue Analogues

Prussian Blue (PB)-type solid	structure	magnetic behavior	critical temperature, T_C (K)	coercive field (Oe)	remnant magnetization ($cm^3\ mol^{-1}$ Oe)
Mn_4Fe_4(title complex)	3D noncubic	canted ferri	14.8	1348 (10 K), 6153 (2 K)	1348 (10 K), 6153 (2 K)
$(RbMn_{1.15})_6Fe_6$[a]	3D cubic	ferri	10	240 (10 K)	240 (10 K)
Mn_4Fe_3[b]	2D	canted ferri	11		
Mn_3Fe_2[c]	2D	meta	6.4	5585 (1.8 K)	5585 (1.8 K)
Mn_2Fe_2[d]	2D	ferri	5.0		
Mn_2Fe_2[d]	2D	antiferro	4.4		

[a] Data taken from ref 11a. [b] Data taken from ref 19c. [c] Data taken from ref 19a. [d] Data taken from ref 21c.

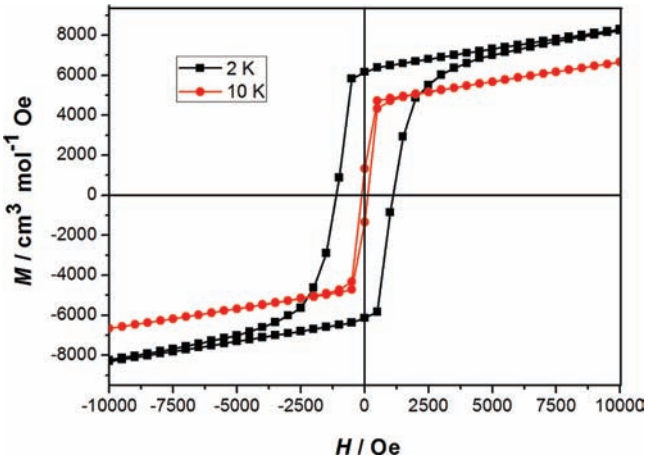

Figure 10. Hysteresis loops at 2 K and 10 K for **1**.

where k_B is the Boltzmann constant, N is the Avogadro constant, g is the mean Landé factor ($g = 2.00$), β is the Bohr magneton, S_{Mn} and S_{Fe} are spin values of individual Mn(II) and Fe(III) ions ($S_{Mn} = {}^5/_2$, $S_{Fe} = {}^1/_2$), and Z_{Mn} and Z_{Fe} are the numbers of nearest metal centers connected to Mn and Fe via cyanide bridges ($Z_{Mn} = Z_{Fe} = 4$). With a T_C value of 14.8 K for **1**, the $|J|$ value is estimated to be 1.04 cm^{-1}. For discrete polynuclear complexes,[14,15c−f,17c,22d,37] and 1D chains,[21a,c] the J values lie within the range of −10 cm^{-1} to 0 cm^{-1}. As shown in Table 3, the exchange interaction parameters $|J|$ for a 2D layer[19a] are deduced using the values of 2.1 cm^{-1} to the $[Fe^{III}(\mu\text{-}CN)_4(CN)_2)]$ center and 1.6 cm^{-1} to the $[Fe^{III}(\mu\text{-}CN)_2(CN)_4)]$ center. The J value of complex **1** is shown to be smaller than the value of the aforementioned 2D cyanides. Because the number of magnetic neighbors around a given metallic center in the 3D cyanide is larger than that in the low-dimensional cyanide, the assembly of Fe(III) and Mn(II) ions in the 3D cyanide creates a long-range ordering magnet. According to Néel,[36b] T_C is proportional to the number of magnetic neighbors around a given metallic center and to the magnitude of the interaction between two centers.[4b] Therefore, the critical temperature ($T_C = 14.8$ K) for **1** is higher than that of the cyanide-bridged 2D[16b,19a,c,21c] and 1D[10] Mn(II)−Fe(III) complexes (below 11 K). The number of magnetic neighbors around a given metallic center affecting T_C could also be used to explain the decrease of T_C among the 2D cyanides (Mn_4Fe_3[19c] > Mn_3Fe_2[19a] > Mn_2Fe_2,[21c] as listed in Table 3). In addition, although the title complex Mn_4Fe_4 has less magnetic neighbors around a given metallic center than the 3D cubic cyanide $(RbMn_{1.15})_6Fe_6$[11a] (see Table 3), it shows a higher T_C, a larger coercive field, and more remnant magnetization, which should be attributed to the larger magnetic anisotropy induced by the noncubic framework of **1**. Such influence of the magnetic anisotropy could also explain the fact that, in Table 3, the 3D cubic cyanide $(RbMn_{1.15})_6Fe_6$ with more magnetic neighbors around a certain metallic center is of lower T_C, smaller coercive field, and less remnant magnetization than that of the 2D Mn_4Fe_3[19c] or Mn_3Fe_2[19a] cyanide. In short, more magnetic neighbors around a given metallic center of larger magnetic anisotropy would result in a higher T_C, larger coercive field, and more remnant magnetization.

Conclusion

A hybrid cyanide-bridged three-dimensional (3D) compound that presents a new molecule-based ferrimagnet has been obtained, providing a feasible route to design and prepare new 3D cyanide-bridged complexes. After comparing the different dimensional FeMn cyanides, the detail magnetostructural correlation is drawn: More magnetic neighbors around a given metallic center of larger magnetic anisotropy would result in a higher T_C, larger coercive field, and more remnant magnetization. This magnetostructural correlation is valuable to the further design and investigation of cyanides. In particular, its well-defined composition and structure offered a meaningful model system for theoretical work in molecular magnetism and for application in functional materials.

Acknowledgment. This work was financially supported by the Natural Science Foundation of China (Grant Nos. 20731002 and 20971019) and the Fundamental Research Funds for the Central Universities, and Open Project of State Key Laboratory of Supramolecular Structure and Materials (No. SKLSSM201004).

(37) (a) Kim, J.; Han, S.; Cho, I. K.; Choi, K. Y.; Heu, M.; Yoon, S.; Suh, B. J. *Polyhedron* **2004**, *23*, 1333–1339. (b) Tanase, S.; Andruh, M.; Stanica, N.; Mathoniere, C.; Rombaut, G.; Golhen, S.; Ouahab, L. *Polyhedron* **2003**, *22*, 1315–1320. (c) Wang, S.; Zuo, J. L.; Zhou, H. C.; Song, Y.; You, X. Z. *Inorg. Chim. Acta* **2005**, *358*, 2101–2106.